Investigation of the Local Structure and Dynamics of the H Subunit of the Mitochondrial Glycine Decarboxylase Using Heteronuclear NMR Spectroscopy†

Laure Guilhaudis,‡ Jean-Pierre Simorre,*,‡ Martin Blackledge,‡ Michel Neuburger,§ Jacques Bourguignon,§ Roland Douce,§ Dominique Marion,‡ and Pierre Gans‡

Institut de Biologie Structurale "Jean-Pierre Ebel" (CEA-CNRS), 41 rue Jules Horowitz, 38027 Grenoble Cédex 1, France, and Département de Biologie Moléculaire et Structurale, Laboratoire de Physiologie Cellulaire Végétale (CNRS URA n° 576), CEA-Grenoble, 38054 Grenoble Cédex 9, France

Received February 22, 1999; Revised Manuscript Received April 21, 1999

ABSTRACT: The lipoate-dependent H protein plays a pivotal role in the catalytic cycle of the glycine decarboxylase complex (GDC), undergoing reducing methylamination, methylene transfer, and oxidation. The local structure and backbone dynamics of the methylamine-loaded H (Hmet), oxidized H (Hox), and H apoprotein (Hapo) have been investigated in solution. Filtered NOESY experiments using a [^{13}C]Hmet as well as comparison of the heteronuclear shifts between the Hox and Hmet proteins demonstrate that the methylamine group is located inside a cleft of the protein. Furthermore, this group appears to be locked in this configuration as indicated by the high value of the activation energy (37 kcal/mol) of the global unloading reaction and by its restricted mobility, deduced from ^{13}C relaxation measurements. Comparisons of the ^{1}H and ^{15}N chemical shifts and ^{15}N relaxation in the three forms suggest that part of the lipoyl−lysine arm interacts with the protein polypeptide in the Hox and Hmet. The major change induced by the loading of the methylamine group concerns the C-terminal helix whose mobility becomes completely restricted compared to those of the Hox and Hapo. This C-terminal helix exhibits different reorientational characteristics in the three forms, which can be explained in the Hapo by a model consisting of a twisting motion about an axis passing through the helix. Our results indicate that the model of a freely swinging arm proposed for other lipoate-containing proteins is not acceptable in solution for the GDC. The implication of this observation in terms of the mechanism of the interaction of the H protein with the T protein, its physiological partner during the catalytic cycle, is discussed.

In plant and mammalian mitochondria (*1*, *2*), the glycine decarboxylase complex catalyzes the oxidative decarboxylation of glycine in a multistep reaction. As its mammalian counterpart, this complex consists of four different component enzymes designated as the P protein (a homodimer containing pyridoxal phosphate, 200 kDa), the H protein (a monomeric lipoamide-containing protein, 14 kDa), the T protein (a monomeric protein requiring tetrahydropteroyl glutamate cofactor, 45 kDa), and the L protein, a dihydrolipoamide dehydrogenase (a homodimer containing FAD and a redox active cystine residue, 100 kDa). All the protein components of the glycine decarboxylase system dissociate very easily and behave as nonassociated proteins following mitochondrial inner membrane rupture. Under these conditions, the H protein acts as a mobile substrate that commutes successively between the other three proteins (*3*, *4*) (Figure 1). The P protein catalyzes the decarboxylation of the glycine molecule, and the remaining methylamine moiety is passed to the distal sulfur of the lipoamide cofactor of the H protein. The T protein then interacts with the methylamine-loaded H protein and catalyzes the deamination and the transfer of the methylene carbon to its tetrahydrofolate−polyglutamate cofactor, forming methylenetetrahydrofolate−polyglutamate. Finally, the L protein catalyzes the reoxidation of the lipoamide cofactor.

Recent structural studies have brought new insight to the understanding of the mechanisms employed by the H protein in carrying out its complex functional activity. High-resolution structures of the oxidized (Hox)[1] and the methylamine-loaded (Hmet) forms from pea leaf mitochondria (*5*, *6*) show that the lipoate cofactor is attached by an amide

† This work has been supported by the Centre National de la Recherche Scientifique, the Commissariat à l'Energie Atomique. This is publication n° 617 of the Institut de Biologie Structurale "Jean Pierre Ebel". L. Guilhaudis was a recipient of a MESR fellowship.

* To whom correspondence should be addressed. E-mail: jps@rmn.ibs.fr. Telephone: (33) 4 76 88 57 99. Fax: (33) 4 76 88 54 94.

‡ Institut de Biologie Structurale "Jean-Pierre Ebel" (CEA-CNRS).

§ CEA-Grenoble.

[1] Abbreviations: 1D, one-dimensional; 2D, two-dimensional; CH_2H_4-$FGlu_n$, N^5N^{10}-methylenetetrahydrofolate−polyglutamate; DSS, 2,2-dimethyl-2-silapentane-5-sulfonate, sodium salt; GARP, globally optimized alternating-phase rectangular pulses; GDC, glycine decarboxylase complex; Hapo, unlipoylated form of the H protein; H_4Fglu_n, tetrahydrofolate−polyglutamate; Hmet, H protein loaded with methylamine; $Hmet_{[^{13}C,^{15}N]}$, Hmet protein loaded with [^{13}C,^{15}N]methylamine; Hox, oxidized lipoylated form of the H protein; Hred, reduced lipoylated form of the H protein; HSQC, heteronuclear single-quantum coherence spectroscopy; IPTG, isopropyl β-D-thiogalactopyranoside; L, dihydrolipoamide dehydrogenase; LPL, lipoate-protein-ligase; NMR, nuclear magnetic resonance; NOE, nuclear Overhauser effect; NOESY, nuclear Overhauser enhancement spectroscopy; SHMT, serine hydroxymethyltransferase; TCEP, tris(2-carboxyethyl)phosphine; TOCSY, total correlated spectroscopy; TPPI, time-proportional phase incrementation; WALTZ-17, wideband alternating-phase low-power technique for zero residual splitting; WATERGATE, water suppression by gradient-tailored excitation.

10.1021/bi990422p CCC: $18.00
Published on Web 06/06/1999

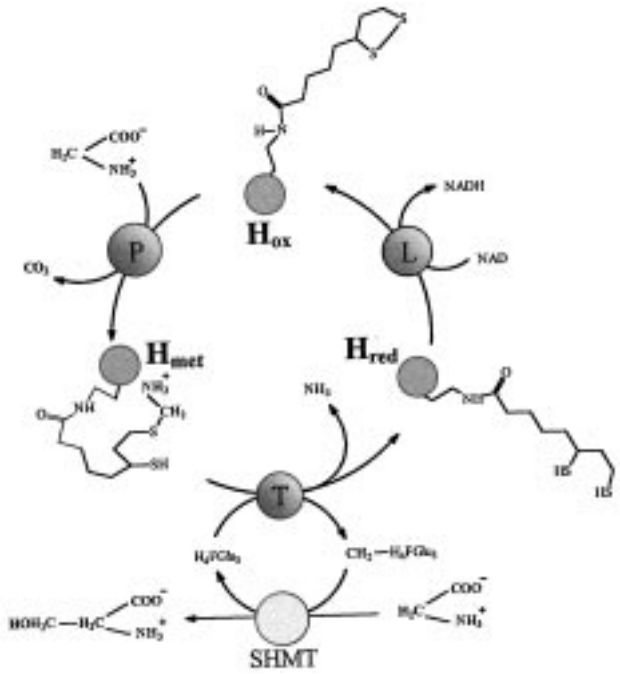

FIGURE 1: Scheme outlining the reactions involved in the oxidative decarboxylation and deamination of glycine in plant mitochondria. P, T, H, and L are the protein components of the glycine decarboxylase complex. The serine hydroxymethyltransferase (SHMT) is involved in the recycling of methylenetetrahydrofolate−polyglutamate ($CH_2H_4FGlu_n$, where *n* is the number of glutamates) into tetrahydrofolate−polyglutamate (H_4FGlu_n) and the synthesis of serine. Note the central role of the H protein in the reaction mechanism.

linkage to a lysine side chain located in the loop of a hairpin configuration. In its oxidized form, the lipoamide arm is located at the surface of the protein in a rather flexible conformation. Following the methylamine transfer, the cofactor is pivoted to bind into a cleft at the surface of the H protein, locking the lipoamide−methylamine arm (*7*). This conformation, which leaves the methylamine group buried in a mostly hydrophobic environment, is in disagreement with the model of a swinging lipoyl−lysine arm visiting the different catalytic sites as predicted for oxoacid dehydrogenase complexes (*8*, *9*). In the latter case, the lipoamide arm attached to the lipoyl domain of the E2 subunit, which is structurally analogous to the H protein, has total freedom to rotate in the complex (*10*−*12*). Furthermore, the lipoyl E2 domain is attached to the other domains by long and flexible linkers allowing the lipoamide arm to visit the different active sites during catalysis.

With regard to the Hmet, it cannot be excluded that the crystallographic structure represents a conformational energy ground state, and that in solution the methylamine-loaded arm has a higher degree of freedom than in the crystal lattice.

The peptide backbone of the H protein remains unchanged in the apoprotein (Hapo) (*13*) as well as in Hox and Hmet [average rmsd in all the Cα positions of 0.5 Å between Hmet and Hox (*7*)] despite the differential electrophoretic behavior of the Hox and Hmet proteins (*14*). Consequently, the specific functional behavior of the various lipoylated forms of the protein suggests that the molecular recognition between the H protein and its reaction partners may implicate differential local mobility of the molecule in its different ligation states.

It is therefore of interest to investigate the structure and dynamics of the various functional forms of H protein in the solution state. We present here an NMR investigation of the local structural changes induced by the presence or absence of the lipoamide factor by comparison of the heteronuclear chemical shifts of the Hox, Hmet, and Hapo. The behavior of the lipoamide arm has been characterized using heteronuclear relaxation and filtered NOESY experiments to determine the structure and dynamics of the cofactor relative to the peptide chain. Finally, the local and global dynamics of the three forms of the protein are compared in detail using ^{15}N relaxation, to provide a possible explanation for the differential physicochemical properties of the three forms. In view of the mobile nature of the GDC complex, this information is essential for the understanding of the mechanisms of protein−protein interaction within the complex, and is complementary to the high-resolution structural information that is already available.

MATERIALS AND METHODS

Protein Production and Labeling

Unlabeled Hox was overproduced in *Escherichia coli* using a Luria-Bertani medium supplemented with 150 μM lipoic acid and was purified following the procedure described by Macherel et al. (*13*). The Hox protein was then loaded with methylamine using [^{13}C,^{15}N]glycine (Sigma) as a starting reagent as described by Neuburger et al. (*14*) with minor modifications. Twenty milligrams of Hox was incubated in 1 mL of a buffered solution consisting of 10 mM potassium phosphate and 10 mM Mops (pH 7.5) supplemented with 1 mM $MgCl_2$, 20 μM pyridoxal phosphate, and 2 μM P protein. Dihydrolipoamide dehydrogenase (L protein from pea leaf mitochondria, 0.1 μM) and NAD^+ (0.5 mM) were added to the medium to oxidize the reduced form of the H protein (Hred) which may be present. The reaction was started by adding 40 mM [^{13}C,^{15}N]glycine. The rate of Hmet formation was followed spectrophotometrically using the TCEP assay described below.

Uniformly ^{15}N-labeled Hapo was obtained by growing the *E. coli* cells on a M9 minimal medium containing 1 g/L [^{15}N]ammonium chloride (Isotec) as the sole nitrogen source. Expression of the protein was induced with 0.4 mM IPTG when the *E. coli* culture reached an optical density (A_{600nm}) of ∼0.5. After incubation for 3 h at 37 °C under agitation, the bacterial suspension was cooled on ice before centrifugation (5000*g* for 15 min). The H apoprotein was then released from bacteria by three cycles of freezing and thawing and purified as described in ref *13*. Approximately 15 mg of purified apoprotein was obtained per liter of culture medium. Lipoylation of the apoprotein was carried out in vitro using *E. coli* lipoate-protein-ligase (*15*, *16*) as described by Gueguen et al. (*17*). *E. coli* strain TM 202 harboring the recombinant plasmid TM 70 containing the *lplA* gene encoding LPL was kindly provided by J. E. Cronan (University of Illinois, Urbana, IL). *E. coli* LPL was overexpressed as described by Green et al. (*16*) and purified as described by Gueguen et al. (*17*). Apoprotein (40 mg) was incubated for 2 h at 37 °C in the presence of 5 mM ATP, 10 mM lipoic acid, 5 mM $MgSO_4$, and 20 μM LPL in 10 mM Tris and 10 mM Mops (pH 7) in a total volume of 1 mL. The loading of Hox with [^{13}C,^{15}N]methylamine was

carried out as described above. The lipoylation and the methylamine loading of the H protein were checked by mass spectrometry. The [^{15}N]Hapo, [^{15}N]Hox, and [^{15}N]Hmet proteins were purified following the procedures described by Neuburger et al. (*14*) and Macherel et al. (*13*).

Protein concentrations were determined either by UV spectroscopy from the absorbency at 205 nm of the peptide bond using a molar extinction coefficient of 4.34×10^5 cm^{-1} M^{-1} or by the TCEP test described below.

Stability of the Methylamine Group with Temperature

Assays were performed using 0.1 mM Hmet in 0.5 mL of 50 mM phosphate buffer at pH 7 unless otherwise stated. The samples were stored at 15, 18, 32, 40, and 50 °C. The assay at 18 °C was carried out at pH 5.5. We have verified by circular dichroism measurements that the H protein stored up to 60 °C was still folded and did not lose its catalytic properties in a reconstituted GDC (M. Neuburger, unpublished data). At different times, aliquots were removed and cooled on ice and the release of the unloaded H protein was assessed using the TCEP test described below. The initial H protein concentration in the incubation medium was determined by completely unloading the Hmet protein with 1 μM T protein and 0.5 mM H_4Fglu_1.

The H protein concentration was determined according to Neuburger et al. (*18*). In the presence of NAD$^+$, dihydrolipoamide dehydrogenase catalyzes the oxidation of the SH groups of lipoamide into the disulfide bond with the formation of NADH. A large excess of TCEP [$(R)_3P$] allows rapid chemical reduction of the disulfide bond of the lipoamide without affecting kinetic properties of both proteins:

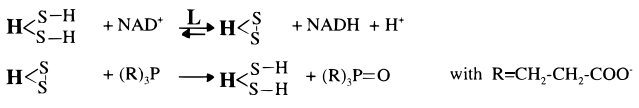

For low concentrations of H protein (<4 μM), the initial rate of NADH production is directly proportional to the amount of H protein (either oxidized or reduced) present in the assay medium. Therefore, using a calibration curve (rate of NADH formed vs H protein concentration), it is possible to determine the concentration of H protein in the reaction medium.

Measurements were taken at 30 °C in 0.5 mL of 50 mM Mops (pH 7.5) containing the sample, 8 mM TCEP, 3 mM NAD$^+$, and 40 μg of dihydrolipoamide dehydrogenase (from pig heart, Sigma). The rate of NAD$^+$ reduction was followed at 340 nm, using a Kontron Uvikon-810 spectrophotometer. This technique allows discrimination of Hox and Hred from Hmet as the latter does not react with either the L protein (or dihydrolipoamide dehydrogenase from pig heart) or TCEP in the coupled assay.

NMR Spectroscopy

Sample Preparation. H protein loaded with [^{13}C,^{15}N]-methylamine (Hmet$_{[^{13}C,^{15}N]}$) was dissolved at a concentration of 3.5 mM in 50 mM phosphate buffer (pH 5.5) and 0.2% sodium azide in 90% H_2O/10% D_2O. This sample was also lyophilized in D_2O. Hapo, Hox, and Hmet labeled with ^{15}N were prepared for NMR experiments in 50 mM phosphate buffer (pH 5.5), 0.1 mM EDTA, and 0.2% sodium azide in 90% H_2O/10% D_2O at a protein concentration of 1 mM (Hapo), 1.3 mM (Hox), and 2 mM (Hmet).

NMR Experiments. All NMR experiments were carried out on a Bruker AMX-600 NMR spectrometer equipped with a triple-resonance (^{1}H, ^{13}C, and ^{15}N) probe including shielded *z*-gradients. NMR experiments were performed at 18 °C unless otherwise stated. 2D TOCSY (*19*, *20*) and 2D NOESY (*21*, *22*) experiments were carried out with the Hmet$_{[^{13}C,^{15}N]}$ samples dissolved in 90% H_2O/10% D_2O and in 99% D_2O. TOCSY spectra were acquired with a WALTZ-17 isotropic mixing time of 60 ms, including the delays of the clean TOCSY pulses and with a spin lock field strength of 10 kHz. The NOESY mixing times were set to 180 ms in H_2O and 140 ms in D_2O. The total experimental time of the 2D experiments was set to 24 h. 2D ^{1}H−^{15}N HSQC (*23*) experiments were performed with the three ^{15}N-labeled samples of the H protein with a spectral resolution of 13.9 Hz in t_1 and 9.4 Hz in t_2, eight transients, and a total experimental time of 1 h. 2D ^{1}H−^{13}C HSQC and 2D ^{1}H−^{13}C HSQC−NOESY (*24*) experiments were carried out with the Hmet$_{[^{13}C,^{15}N]}$ samples. The NOE mixing times were set to 80 and 140 ms for experiments carried out with 90% H_2O/10% D_2O samples and 140 ms for the experiment carried out in D_2O. The experimental times of the HSQC and the HSQC−NOESY experiments were 90 min and 48 h, respectively. Water suppression was achieved using the pulsed-field gradient-based WATERGATE method (*25*) except for the TOCSY experiment where a combination of low-power presaturation and a jump and return read pulse (*26*) was used. Quadrature detection in the indirect frequency dimensions was achieved using the States−TPPI method (*27*). ^{15}N and ^{13}C were decoupled using the GARP sequence (*28*) with field strengths of 1.9 and 2.1 kHz, respectively. Proton chemical shifts were reported with respect to the H_2O signal relative to DSS taken to be 4.8483 ppm at 18 °C and pH 5.5. The ^{15}N and ^{13}C chemical shifts were referenced indirectly using the ^{1}H/X frequency ratios of the zero point: 0.101329118 (^{15}N) and 0.251449536 (^{13}C) (*29*). The spectra were processed using FELIX version 95.0 (MSI Technologies).

^{13}C T_1, $T_{1\rho}$, and ^{13}C{^{1}H} NOE measurements for the methylamine group were performed using ^{13}C 1D experiments. Experiments were carried out with the Hmet$_{[^{13}C,^{15}N]}$ sample dissolved in 90% H_2O/10% D_2O. For ^{13}C T_1 and $T_{1\rho}$, a refocused INEPT sequence (*30*, *31*) was included prior to the relaxation delay to improve the sensitivity. The delays of the refocused INEPT were optimized for CH_2 groups. During the T_1 and $T_{1\rho}$ relaxation delays, proton decoupling was applied to suppress cross-correlated relaxation effects. T_1 measurements were recorded with 11 relaxation delays of 1, 20, 50, 100, 200, 400, 600, 800, 1000, 1250, and 1500 ms, while $T_{1\rho}$ experiments were recorded with eight relaxation delays of 1, 5, 10, 15, 20, 30, 40, and 50 ms. A recycle delay of 3.5 s between transients was used to ensure sufficient recovery of ^{1}H magnetization. For $T_{1\rho}$ experiments, a spin lock field of 2.5 kHz was used at the frequency of the ^{13}C resonance of the methylamine group. A total of 2048 complex points were acquired with 512 (T_1 and $T_{1\rho}$) or 64 (NOE) transients.

^{15}N relaxation experiments were performed with the ^{15}N-labeled samples of the three forms of the H protein. The

pulse sequences used for ^{15}N T_1, $T_{1\rho}$, and $^{15}N\{^1H\}$ NOE experiments were similar to those reported previously (*32*). Sensitivity-enhanced 2D $^1H-^{15}N$ correlation spectra were acquired using pulsed field gradients to select for coherence transfer pathways (*33*, *34*) and the water-flip back method (*32*). For T_1 measurements, eight delays of 20, 60, 150, 250, 400, 600, 800, and 1190 ms were used, while for $T_{1\rho}$, seven delays of 20, 40, 60, 80, 120, 160, and 200 ms were used. The recycle delay was set to 2.5 s. In the $T_{1\rho}$ experiments, a spin lock field of 2.5 kHz was applied. T_1 and $T_{1\rho}$ experiments were recorded using eight transients per t_1 increment and with a spectral resolution of 17.8 Hz in t_1 and 9.4 Hz in t_2, and 13.9 Hz in t_1 and 9.4 Hz in t_2, respectively. NOE data were collected with 64 transients and with a spectral resolution of 13.9 Hz in t_1 and 9.4 Hz in t_2.

For each series of ^{13}C or ^{15}N relaxation experiments, the order of the relaxation delays was chosen randomly in case of possible systematic instrumental drift. To ensure a constant temperature, off-resonance ^1H irradiation with different durations was applied during the recycle delay. ^1H (^{13}C relaxation) and ^{15}N (^{15}N relaxation) were decoupled using a WALTZ-16 sequence (*35*) at a field strength of 2.8 kHz and a GARP scheme with a field strength of 1.9 kHz, respectively. For $^{13}C\{^1H\}$ and $^{15}N\{^1H\}$ NOE, ^1H saturation was achieved using a WALTZ-16 sequence. The ^1H saturation was applied for 3.5 s at a field strength of 2.8 kHz for $^{13}C\{^1H\}$ NOE and for 3 s at a field strength of 2.3 kHz for $^{15}N\{^1H\}$ NOE. The delay between transients was set to 3.5 and 5 s for the $^{13}C\{^1H\}$ NOE and $^{15}N\{^1H\}$ NOE, respectively. The steady-state NOE spectra, with and without ^1H saturation, were recorded in an interleaved manner.

Relaxation Data Processing and Analysis

The ^{13}C relaxation data were multiplied by an exponential apodizing function, and a baseline correction was applied for accurate determination of peak intensity. R_1 and R_2 relaxation rates were extracted using a Levenberg−Marquardt nonlinear least-squares fit of the intensities with a three-parameter monoexponential function. Standard deviations in the optimized parameters obtained from the nonlinear fitting procedure were used to estimate errors on relaxation rates. The $^{13}C\{^1H\}$ NOE was calculated from

$$\mathrm{NOE} = \left(\frac{I_{\mathrm{sat}}}{I_{\mathrm{ref}}} - 1\right) \tag{1}$$

where I_{sat} and I_{ref} are the intensities corresponding to spectra with and without ^1H saturation, respectively. The uncertainty in the NOE value was calculated from the peak intensity measurements estimated from the root-mean-square (rms) baseline noise of both spectra.

For the ^{15}N relaxation, data were transformed using a skewed sine bell (T_1 and $T_{1\rho}$) squared window or a Gaussian (NOE) apodizing function, and the residual water suppression was achieved using a sine bell convolution. For the^{15}N T_1, $T_{1\rho}$, or NOE, final dimensions of the matrixes were 2048 × 1024 real points corresponding to a digital resolution of 2.3 (^1H) and 1.7 Hz/point (^{15}N). The data were analyzed following the procedure described previously (*36*).

The measured ^{15}N relaxation rates depend on linear combinations of the spectral density function sampled at different transition frequencies and $J(0)$. In the case of isotropic overall tumbling, the following "model-free" spectral density function was used:

$$J(\omega) = {}^2/_5 S_2{}^2\left[S_1{}^2\frac{\tau_c}{1+(\omega\tau_c)^2} + (1-S_1{}^2)\frac{\tau'}{1+(\omega\tau')^2}\right] \text{ with } \tau' = \frac{\tau_c\tau_i}{\tau_c+\tau_i} \tag{2}$$

where τ_c is the overall correlation time of the molecule and τ_i is the characteristic correlation time of the internal motion.

In the standard Lipari−Szabo analysis (*37*, *38*), $J(\omega)$ is derived from eq 2 assuming $S_2{}^2 = 1$, and the generalized order parameter $S_1{}^2 = S^2$ then describes the amplitude of the fast internal motion ranging from $S^2 = 0$ for unrestricted motion to $S^2 = 1$ for a fixed vector. It is sometimes necessary to introduce a second internal motion, on a slower time scale in an extended Lipari−Szabo approach (*39*). The correlation time of the rapid librational motion is assumed to be negligible for NMR relaxation, and is only present in the order parameter $S_2{}^2$ ($S^2 = S_1{}^2S_2{}^2$).

The data were initially treated using isotropic overall tumbling. Appropriate models for internal dynamics parameters were chosen using an iterative fitting procedure and statistical significance tests (*36*, *40*). Five models were tested in order of increasing motional complexity: (1) S^2, (2) S^2 and τ_i, (3) S^2 and R_{ex}, (4) S^2, τ_i, and R_{ex}, and (5) $S_2{}^2$, $S_1{}^2$, and τ_i, where τ_i is the internal correlation of the internal motion and R_{ex} is a term accounting for chemical exchange on a slow time scale. Model 5 refers to the extended model with a second internal motion defined by $S_2{}^2 \neq 1$ and τ_i being on the scale of nanoseconds (the fast internal correlation time approaches zero as in model 1).

Data for Hmet were also treated for the general case of anisotropic rotational diffusion of the molecule; the relevant spectral density function for overall tumbling (*41*) is then dependent on the orientation of the NH vector with respect to the principal axes of the rotational diffusion tensor and their component values. The direction and components of the diffusion tensor were fitted to experimental R_2/R_1 ratios using procedures described elswhere (*42*).

The possible collective motion of the C-terminal helix was modeled by replacing the order parameter $S_1{}^2$ in eq 2 with specific geometric models for angular reorientation. For steric reasons, the most appropriate motional models appeared to be either free rotation of the helix about a symmetry axis fixed on the molecule (*43*)

$$S^2 = [P_2(\cos\beta)]^2 \tag{3}$$

where β is the angle made by each vector and the axis of the cone and $P_2(x)$ is the second-order Legendre polynomial [$P_2(x) = (3x^2 - 1)/2$] or restricted rotation about the same angular cone of half-angle β between the limits γ and $-\gamma$ (*38*):

$$S_r{}^2 = [P_2(\cos\beta)]^2 + 3\sin^2\beta\sin^2\gamma(\cos^2\beta + {}^1/_4\sin^2\beta\cos^2\gamma)/\gamma^2 \tag{4}$$

The measured parameters R_2/R_1 and NOE for the helical residues were simultaneously fitted using the spectral density

function in eq 2. The orientation of the axis was optimized with respect to the geometry of amide vectors from a canonical α-helix, described by spherical polar coordinates (θ and ϕ). The function

$$\chi^2 = \sum_n (\{[(R_2^{meas}/R_1^{meas}) - (R_2^{calc}/R_1^{calc})]/\sigma_{R_2/R_1}\}^2 + [(NOE^{meas} - NOE^{calc})/\sigma_\eta]^2) \quad (5)$$

was minimized to derive the collective motional model. The sum is taken over all residues in the helix, and θ and ϕ (and in the case of restricted reorientation γ) are optimized. τ_c is fixed at the isotropic value, and τ_i is optimized for the whole helix in accordance with its reorientation as a rigid body. The two measured parameters fitted here are independent of S_2^2 as they contain only ratios of linear combinations of $J(\omega)$.

Chemical Shift Assignments

The ^{1}H and ^{15}N backbone assignments have been deposited as entries 4336, 4337, and 4338 at the BioMagRes Bank in Madison, WI.

RESULTS

Stability of the Methylamine Group. Preliminary NMR experiments performed with Hmet at 35 °C and pH 7.0 indicated a complete unloading of the methylamine group within a few days with concomitant formation of formaldehyde (not shown). Consequently, we have investigated the temperature dependence of the stability of the methylamine group. Using the TCEP test, we were able to follow the nonenzymatic unloading of the Hmet protein, that is the release of Hred, as a function of time. Figure 2a shows the effect of temperature on the release of Hred. This figure indicates that Hmet is rather stable at room temperature but becomes more and more unstable as the temperature increases. Indeed, at 40 °C, Hmet loses its methylamine group as NH_3 and formaldehyde in only a few hours (results not shown). The unloading rates were determined from the initial slope of the temperature-dependent reaction, and an activation energy E_a of 37 kcal/mol (Figure 2b) was deduced for the global reaction from the Arrhenius law. If it is assumed that the unloading of the methylamine group is due to nucleophilic attack by hydroxyl ions, a decrease of pH should reinforce the Hmet stability. In addition, an acidic pH would also reduce the exchange rate of the amide protons which is favorable for NMR studies. For these reasons, all the NMR experiments were performed at pH 5.5 and 18 °C. Under these conditions, we observed that Hmet was stable over several weeks (data not shown).

Position of the Methylamine Group. The ^{1}H and ^{13}C assignment of the methylamine group ($CH_2NH_3^+$ group) was obtained from a ^{1}H−^{13}C HSQC spectrum acquired for the $Hmet_{[^{13}C,^{15}N]}$ protein in D_2O. Due to the natural abundance of the ^{13}C, the signal from the unlabeled protein is very weak compared to that of the methylamine group and therefore enables an easy assignment of the methylene. The two nondegenerate resonances for the protons of the CH_2 group are shown in Figure 3a. The chemical shift difference (>1 ppm) clearly shows that the two protons have distinct chemical environments. ^{1}H and ^{15}N assignments of the NH_3 were not determined as this group could not be observed in ^{1}H−^{15}N HSQC spectra.

To characterize the exact position of the group relative to the protein, ^{1}H−^{13}C HSQC−NOESY experiments were

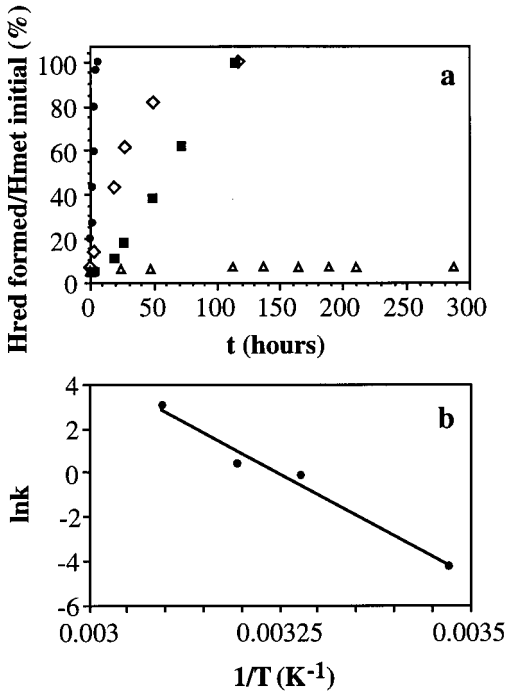

FIGURE 2: Kinetic studies of the unloading reaction of Hmet. (a) Unloading of the Hmet form as a function of time. The temperatures (T) were (△) 15, (■) 32, (◇) 40, and (●) 50 °C. The amount was expressed as a percentage of the total H protein concentration (see Materials and Methods). Aliquots (10−50 μL) of the incubation medium were withdrawn and checked for unloaded H protein formation. The measurements were taken after 0, 24, 48, 113, 137, 164, 189, 210, and 288 h at 15 °C, after 0, 3, 18, 26, 48, 71, and 114 h at 32 °C, after 0, 2.75, 19, 28, 43, 50, and 117 h at 40 °C, and after 0, 25, 50, 75, 145, 200, 260, 290, and 340 min at 50 °C. Panel b shows the Arrhenius plot deduced from the rate constants. The rate constants (k) were extrapolated from the initial slopes of the unloading reaction. The activation energy (E_a) of the overall reaction was calculated to be 37 kcal/mol from the slope according to the equation $\ln k = \ln A - E_a/RT$, where T is the temperature and R the gas constant.

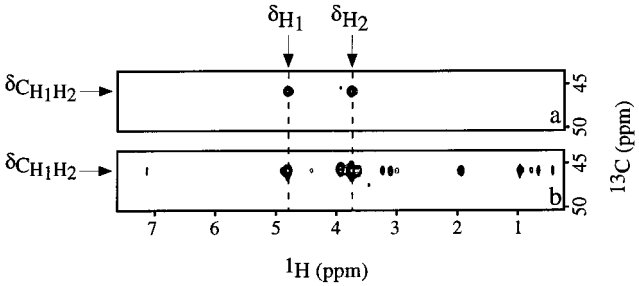

FIGURE 3: Portions of the ^{1}H−^{13}C HSQC (a) and ^{1}H−^{13}C HSQC−NOESY (b) spectra showing the resonance assignment of the CH_2 group of the methylamine and its NOE interactions with the rest of the protein. The ^{1}H and ^{13}C chemical shifts of the CH_2 group are denoted by arrows. The spectra were recorded with the H protein loaded with [^{13}C,^{15}N]methylamine dissolved in D_2O. The ^{1}H−^{13}C HSQC and ^{13}C−^{1}H HSQC−NOESY experiments were carried out with spectral widths of 9091 and 7812 Hz, respectively, for the direct dimension and 15091 Hz in the indirect dimension. Spectra were acquired with 2048 complex points in t_2 and 512 complex points in t_1. The number of transients per t_1 increment was 8 for ^{1}H−^{13}C HSQC spectra and 160 for ^{1}H−^{13}C HSQC−NOESY spectra.

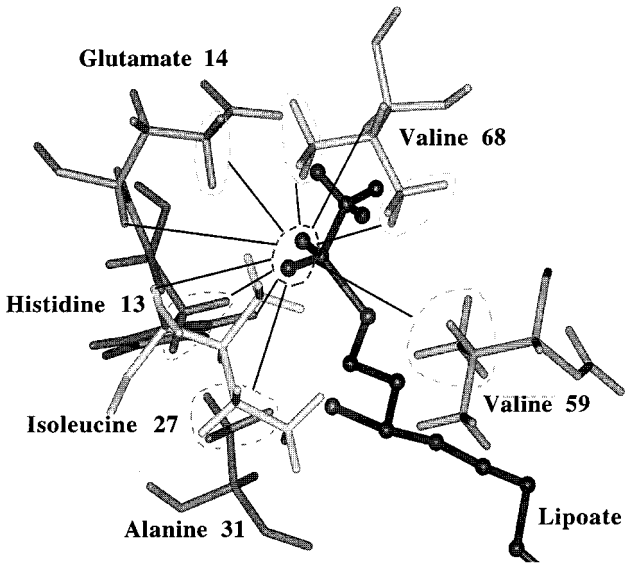

FIGURE 4: View of the cavity region of the Hmet X-ray structure (*6*). The interactions observed in the $^1H-^{13}C$ HSQC−NOESY spectra between the methylamine group and the protein are depicted as black lines. The lipoamide arm and the methylene group are dark gray, and for reasons of clarity, only the protons of the methylamine group are shown. This figure was produced using Insight97 (MSI Technologies).

carried out in H_2O and in D_2O with the $Hmet_{[^{13}C,^{15}N]}$ as well as with the [^{15}N] $Hmet_{[^{13}C,^{15}N]}$ in H_2O. Several correlations between the ^{13}C-labeled methylamine group and protons of the protein were observed in the $^1H-^{13}C$ HSQC−NOESY spectra (Figure 3b). The absence of these cross-peaks in the $^1H-^{13}C$ HSQC results indicated that they corresponded to real NOE transfers. Using 2D TOCSY spectrum, we were able to identify the γ proton resonances of Val68. One correlation at about 7.15 ppm was observed in H_2O and D_2O $^1H-^{13}C$ HSQC−NOESY experiments. This signal remained a singlet in the spectrum recorded with the [^{15}N]$Hmet_{[^{13}C,^{15}N]}$, without ^{15}N decoupling during acquisition, and using 2D NOESY spectra was finally identified as an aromatic proton of His13. As residues 13 and 68 were located near the methylamine group in the crystallographic structure (*6*, *7*), we decided to use the crystallographic structure to resolve some ambiguities concerning other resonance assignments. In the $^1H-^{13}C$ HSQC−NOESY spectrum, we assigned cross-peaks between the CH_2 resonances and the β protons of His13, α and γ of Glu14, α of Ile27, β of Ala31, γ of Val59, and α of Val68. All the interactions observed by NMR are shown in Figure 4, with respect to the X-ray crystal structure (*6*).

For the CH_2 of methylamine, an R_1 of 2.2 ± 0.3 s^{-1}, an R_2 of 86 ± 12 s^{-1}, and an NOE value of 0.20 ± 0.09 were determined. These values are in broad agreement with a correlation time for the methylamine group in the range of 8−10 ns, assuming two independent relaxation sources for the ^{13}C spin due to the different protons and the absence of cross correlation effects.

Structural and Dynamic Comparison of the Three Forms of the H Protein. The chemical shift of a particular nucleus depends on its environment, and the analysis of its variation provides some insights into the residues which undergo an environment change. The chemical shift variations of the backbone amide atoms between the Hapo and the Hox proteins and between the Hox and the Hmet proteins are shown in Figure 5. In Figure 6, only ^{15}N chemical shift changes of >0.5 ppm and ^1H chemical shift changes of >0.1 ppm are shown. These limits were chosen at twice the spectral resolution. Very few changes are found between Hox and Hapo, and only 15% of the proton and nitrogen chemical shift differences are higher than the resolution (panels a and b of Figure 5). The main variations are observed in the loop (Lys63 and Ala64) where the lipoamide arm is attached and for residues Leu35, Gly36, and Glu14 (panels a and b of Figure 6). Additional important variations can be seen between Hox and Hmet in panels c and d of Figure 6. The majority of these variations are found in the hydrophobic pocket, the lipoylation site (Val59−Val62), and the region of His34 and Leu35. Some variations are also observed in the "backside" of the protein for residues Val79, Asn80, Thr81, Thr84, and Trp99 (Figure 6d).

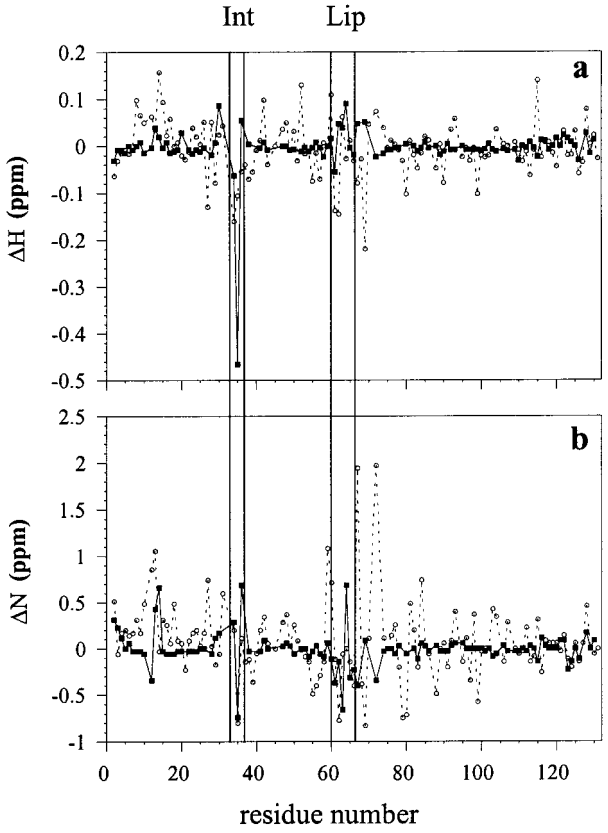

FIGURE 5: Chemical shift differences between the Hapo, Hox, and Hmet proteins. The proton and nitrogen chemical shift differences for Hox − Hmet (○) and Hapo − Hox (■) are displayed in panels a and b, respectively, as a function of the sequence number. The lipoylation site of Glu60−Ser66 (Lip) and the interaction region of Asp33−Gly36 (Int) are denoted by lines. All chemical shifts were determined from two-dimensional $^1H-^{15}N$ HSQC spectra recorded with a spectral resolution of 0.023 ppm/point in the ^1H dimension and 0.15 ppm/point in the ^{15}N dimension.

To compare the backbone dynamics of the three forms of the H protein, ^{15}N R_1, $R_{1\rho}$, and $^{15}N\{^1H\}$ NOE experiments were performed. A total of 112 peaks for nonlipoylated, 107 peaks for Hox, and 116 peaks for Hmet were assigned and sufficiently well resolved for peak intensities to be measured accurately in the R_1, $R_{1\rho}$, and $^{15}N\{^1H\}$ NOE experiments. Thus, R_1, R_2, and NOE data could be obtained for 91% (Hapo), 87% (Hox), and 94% (Hmet) of the 123 protonated backbone ^{15}N atoms. The average errors calculated for R_1

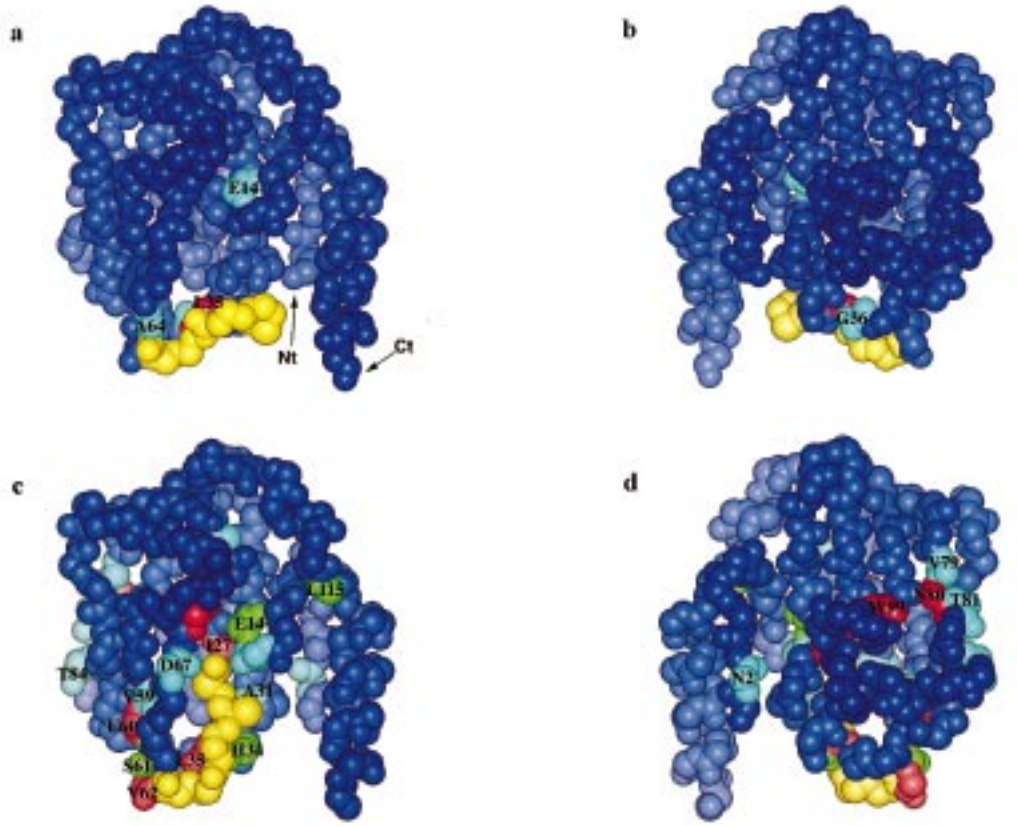

FIGURE 6: Spatial distribution of the chemical shift variations between Hox and Hapo (a and b) and between Hmet and Hox (c and d) shown on the space-filled models (without hydrogen atoms) of the crystallographic structures (*6*). The backside views (b and d) were generated by a rotation of 180° along the *y*-axis of views a and c, respectively. Residues are colored according to the chemical shift change of their backbone amide group (cyan, $\Delta\delta_N > 0.5$ ppm; green, $\Delta\delta_H > 0.1$ ppm; and red, $\Delta\delta_N > 0.5$ ppm and $\Delta\delta_H > 0.1$ ppm). The lipoamide arm is yellow.

Table 1: Summary of Spectral Density Models Used To Fit R_1, R_2, and NOE Data for the Three Forms of the H Protein

optimized parameters	Hapo	Hox	Hmet
model 1 (S^2)	91	94	81
model 2 (S^2 and τ_i)	5	2	9
model 3 (S^2 and R_{ex})	0	1	9
model 4 (S^2, τ_i, and R_{ex})	0	0	4
model 5 (S_2^2, S_1^2, and τ_i)	15	10	11
not fitted	1	0	2
total	112	107	116

were 6.2% (Hapo), 5.1% (Hox), and 2.4% (Hmet), for $R_{1\rho}$ 6.8% (Hapo), 7.4% (Hox), and 3.3% (Hmet), and for NOEs 9.7% (Hapo), 12.6% (Hox), and 4.2% (Hmet). The average uncertainties for R_2 were 6.7% (Hapo), 7.4% (Hox), and 3.2% (Hmet). The R_1, R_2, and NOE values and errors are given in the Supporting Information for the three forms.

The dynamic parameters were initially calculated from the relaxation data assuming isotropic rotational tumbling. Overall correlation times of 8.86 (Hapo), 8.65 (Hox), and 8.96 ns (Hmet) were estimated as described and verified by fitting the average R_2/R_1 ratio of residues present in secondary structural motifs to the calculated value assuming negligible internal motion. The models chosen and the number of residues which fall within each class are summarized in Table 1. The relaxation parameters could be fitted within experimental errors for all but one residue (Lys54) of Hapo and for all but two residues (Ser93 and Leu115) of Hmet. For the majority (81% for Hapo, 88% for Hox, and 70% for Hmet) of the residues, the fit was achieved using the simplest model (model 1).

The average value of the order parameter S^2 for Hapo, Hox, and Hmet is 0.87 ± 0.04, 0.88 ± 0.04, and 0.90 ± 0.02, respectively. There are a number of regions which appear to be disordered ($S^2 < 0.75$) in the three forms (Figures 7 and 8). A common region of internal mobility is the tripeptide (Gly20-Ser21-Val22) connecting the first two strands of the central β sheet. These three residues are characterized by slow internal motions (model 5) of amplitude ($S^2 = 0.5-0.8$) and internal correlation times ranging from 1.03 to 1.34 ns in the three forms of the molecule. The Hapo protein exhibits significant slow motion ($S_1^2 \approx 0.7$ or $\tau_i > 1.0$ ns) for three residues in the short helix region (Asp29−Leu35) and for four residues in the ligand-bearing β strand (Gly57−Asp67). These regions form two sides of the hydrophobic pocket containing the ligand in the Hmet and Hox forms.

Direct comparison of the motional parameters present in the three forms of the molecule is complicated by the higher precision available for the Hmet data set. More complex motional models may be required to achieve statistical significance due to the smaller relative uncertainties of the Hmet relaxation rates. Multiplication of the uncertainty in the Hmet relaxation data by a factor of 2 raises the error to the level of the other two forms and provides a control comparison of the motional parameters. Using this treatment, only the region of Gly20−Val22, the C-terminal residue, and

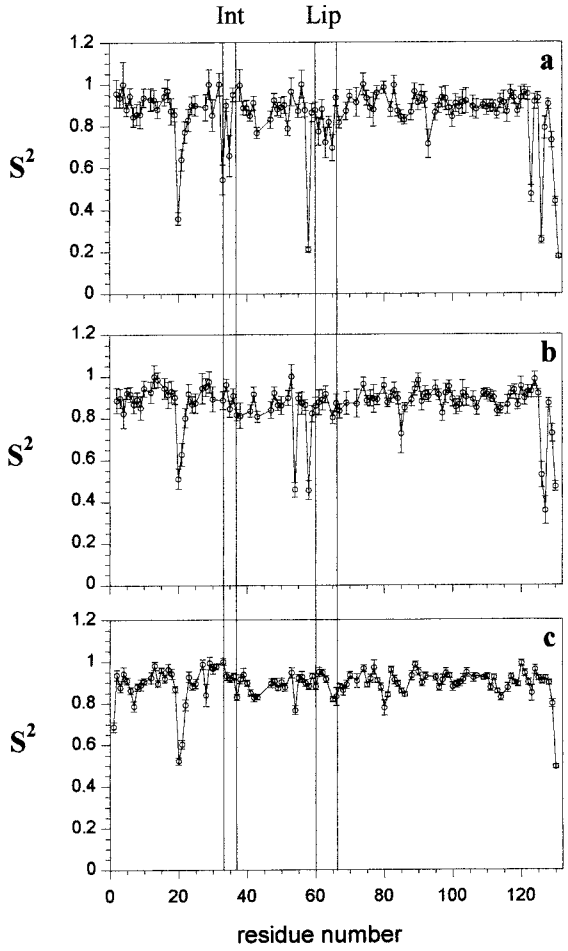

FIGURE 7: Order parameter S^2 of the $^{15}N-^{1}H$ vectors as a function of the sequence number for the different forms of the H protein: Hapo (a), Hox (b), and Hmet (c). The lipoylation site of Glu60−Ser66 (Lip) and the region of Asp33−Gly36 (Int), the zone of interaction between the arm and the polypeptide observed in both Hox and Hmet X-ray structures (*6*, *13*), are denoted by lines.

Lys54 require models more complex than a simple S^2 (model 1).

The C-terminal helix exhibits starkly different reorientational characteristics in the three forms. In Hmet, this helix is rigid and exhibits little internal mobility, while the other two forms exhibit significant motion. In the case of the Hapo, this is characterized by slow internal correlation times on the same order (945−1700 ps) and large amplitude movements for residues Phe123, Glu126, Glu127, Ala129, Ala130, and His131. Similar movements are seen for the Hox except that the Phe123 is rigid.

The S^2 profile of the C-terminal residues in Hapo, shown in Figure 7, exhibits a periodicity similar to that of an α helix ($n = 3-4$), raising the possibility that the structural motif remains intact, but reorients as a rigid unit with respect to the molecular frame. We have therefore attempted to fit the NOE and the ratio of the relaxation rates directly using an explicit geometric model in place of S^2. We have retained the extended Lipari−Szabo formalism and optimized the orientation of the unique axis attached to the molecular frame about which the helix would rotate, and the common internal correlation time characterizing this motion.

If this reorientation proceeds about an axis parallel to vectors on one side of the helix, no relaxation due to this motion will result, as no angular reorientation has been performed by these vectors. Vectors on the other side of the helix will undergo a reorientation with an amplitude of $\pm 2\lambda$, where λ is the angle made by an NH vector and the axis of the helix, and consequently experience differential relaxation. The results (Figure 9) show that the relaxation behavior can be explained by a reorientation of the whole helix about an axis parallel to a subset of the NH vectors. In the optimal orientation, the helix axis makes an angle of 13° with respect to the axis of rotation. The most appropriate movement is described by a twisting of the helix about an eccentric axis passing through the helix. A structure describing this motion is shown in Figure 10. The optimal amplitude of the restricted diffusion on the surface of a cone (γ) approached 90°, and the unrestrained fit was not significantly different.

For Hapo and Hox, no chemical exchange contribution (R_{ex}) was needed except for a 1.42 Hz term for one amino acid (Glu37) in the oxidized form. For Hmet, 13 residues required a chemical exchange contribution of ≤1.7 Hz, and none when the error was increased to the level of the other forms. The larger number of residues fitted with an exchange contribution can therefore be attributed in part to the higher-quality spectra obtained for the relaxation parameters for this form.

Fifteen residues for Hapo, 10 for Hox, and 11 for Hmet required the extended model (*39*) and were fitted with an internal correlation time τ_s of >0.5 ns. In general, these residues correspond to mobile residues with low-order parameters except in the case of Hmet, where four of the 11 residues which required the extended model have high-order parameters ($S^2 > 0.89$) and are located in α helices or β sheets. Eight of the residues modeled with exchange contributions for the Hmet are also present in secondary structural motifs. These observations, and the slightly anisotropic form of the molecule, convinced us that we should investigate the rotational diffusion anisotropy of the protein.

Rotational Diffusion Tensor. The relaxation data for the methylated form were used to determine the rotational diffusion tensor. R_2/R_1 ratios from 67 residues present in α helices or β sheets were initially taken into account. This resulted in a fit of the rotational diffusion tensor which was not statistically justifiable with respect to estimated uncertainty. Inspection of the fitted data revealed that this was mainly due to the ill-fitting C-terminal helix which presented high residual χ^2 terms. Removal of these residues from the data set resulted in a statistically significant fit and significant improvement with respect to the isotropic fit of the same vectors (χ^2). The resulting tensor is nevertheless only slightly anisotropic, with eigenvalues (D_{xx},D_{yy},D_{zz}) of (17.4,18.7,19.8) μs^{-1}, compared to the best fit tensor (incorporating a 3.0 Å thick shell of water) calculated using hydrodynamic modeling of (16.4,18.2,20.6) μs^{-1}. The less precise data sets from Hapo and Hox did not permit differentiation between anisotropic and isotropic rotational diffusion tensors. Not surprisingly, the fits of internal mobility using this tensor to describe overall reorientation are not significantly different from those derived using the isotropic model (data not shown).

DISCUSSION

Location of the Lipoic Arm in the Hmet and Hox Forms. The lipoamide arm plays a crucial role in the reaction

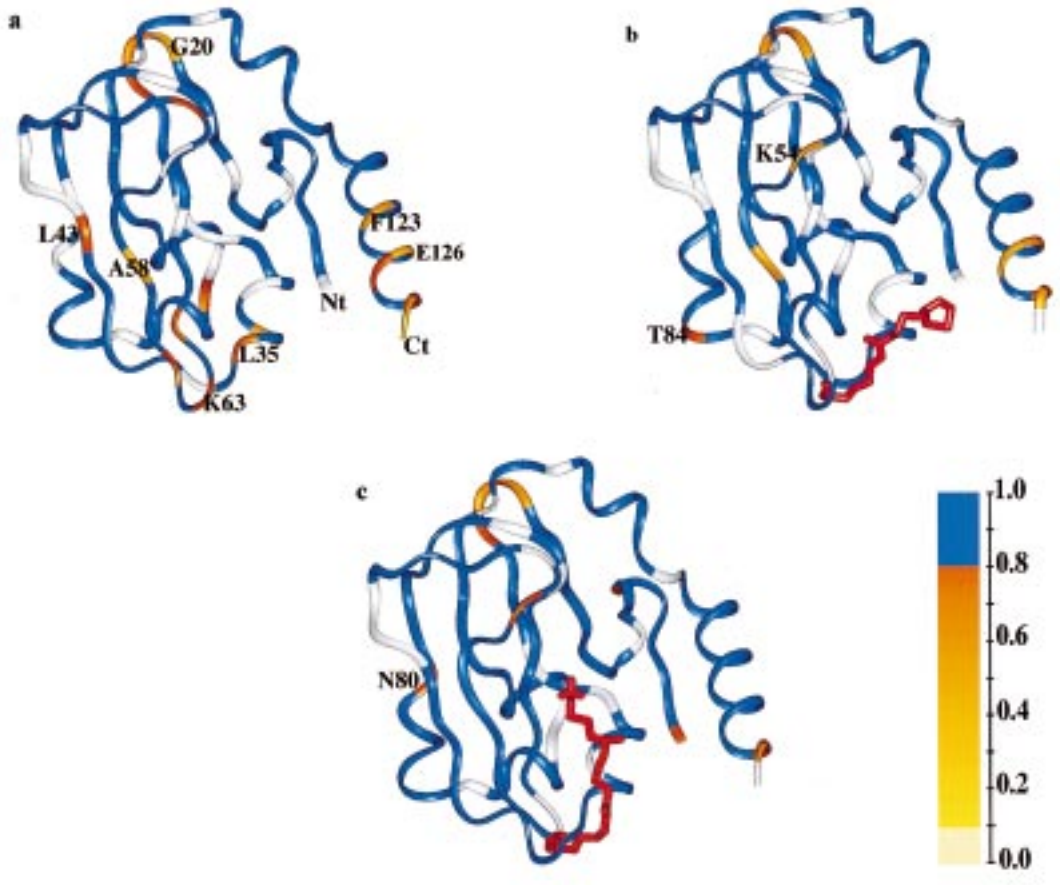

FIGURE 8: Spatial distribution of the order parameter S^2 of the $^{15}N-^{1}H$ vectors for the different H protein forms: Hapo (a), Hox (b), and Hmet (c). Residues are colored according to their S^2 value. The white residues are those for which the dynamic parameters were not determined. The lipoamide arm is red. The distributions are mapped on the crystallographic structures (*6*, *13*).

mechanism of the glycine decarboxylase complex as it is responsible for substrate channelling among the three successive active sites (Figure 1). Consequently, information about its location and dynamic behavior is very important in understanding the complex mechanism. The results obtained by crystallography suggest that the arm is not freely swinging in the case of the GDC, an observation in marked contrast with reports concerning the 2-oxoacid dehydrogenase complexes where spin-labeling experiments have shown that the lipoamide arm has virtually unrestricted motion (*10*, *11*). It is conceivable that the results obtained for the Hox and Hmet forms are due to packing in the crystal lattices and that a different situation prevails in solution.

In the Hmet form, $^{1}H-^{13}C$ HSQC and $^{1}H-^{13}C$ HSQC−NOESY spectra clearly show that the methylamine group is not free to move. Indeed, the chemical shift difference of 1.1 ppm between the two protons of the methylene (CH_2) group as well as the numerous NOEs between these protons and protons of the protein indicates that the methylamine group is bound to the protein. The observation of $^{1}H-^{1}H$ NOE correlations between the methylamine group and some residues located in the cavity [His13, Glu14, Ile27, Ala31, Val59, and Val68 (Figure 4)] strongly suggests that the methylamine group is located as observed by crystallography. Moreover, most of the chemical shift variations between Hmet and Hox concern not only residues located in the cavity but also residues in contact with the lipoic arm itself [His34, Leu35, Glu60, Ser61, Val62, and Asp67 (see panels c and d of Figure 6)].

However, these observations offer little information concerning the mobility of the group, and it was still not clear whether the arm is free to leave the pocket. The fact that the correlation time of the methylamine estimated from the ^{13}C relaxation rate is in the range 8−10 ns and is thus quite similar to the overall correlation time of the protein (about 9 ns) determined using ^{15}N relaxation indicates that the methylene group does not have mobility independent of the protein and would therefore appear to be locked in the pocket. In addition, the very high value found for the activation energy of the unloading reaction indicates that the methylamine group is in a very stable configuration. Such a stable configuration should prevent the carbon unit of the methylamine from nucleophilic attack by hydroxyl ions.

For Hox, we did not have a probe such as the [^{13}C,^{15}N]-methylamine group for obtaining exact information on the location of the oxidized lipoamide arm as ^{13}C-labeled lipoic acid was not available. However, the analysis of chemical shift variations between Hox and Hapo may provide some insight into the residues which undergo a change when the protein is lipoylated. As shown in panels a and b of Figure 6, in addition to the lipoylation site, the region of Leu35-Gly36 is also affected by the presence of the prosthetic group. The crystallographic study of the Hox protein indicates that the lipoamide arm is localized on one side of the protein pointing toward His34. As the arm is stabilized by only one van der Waals contact with His34 and mainly by contacts between symmetrically related molecules, it has been suggested (*5*) that these intermolecular contacts are responsible

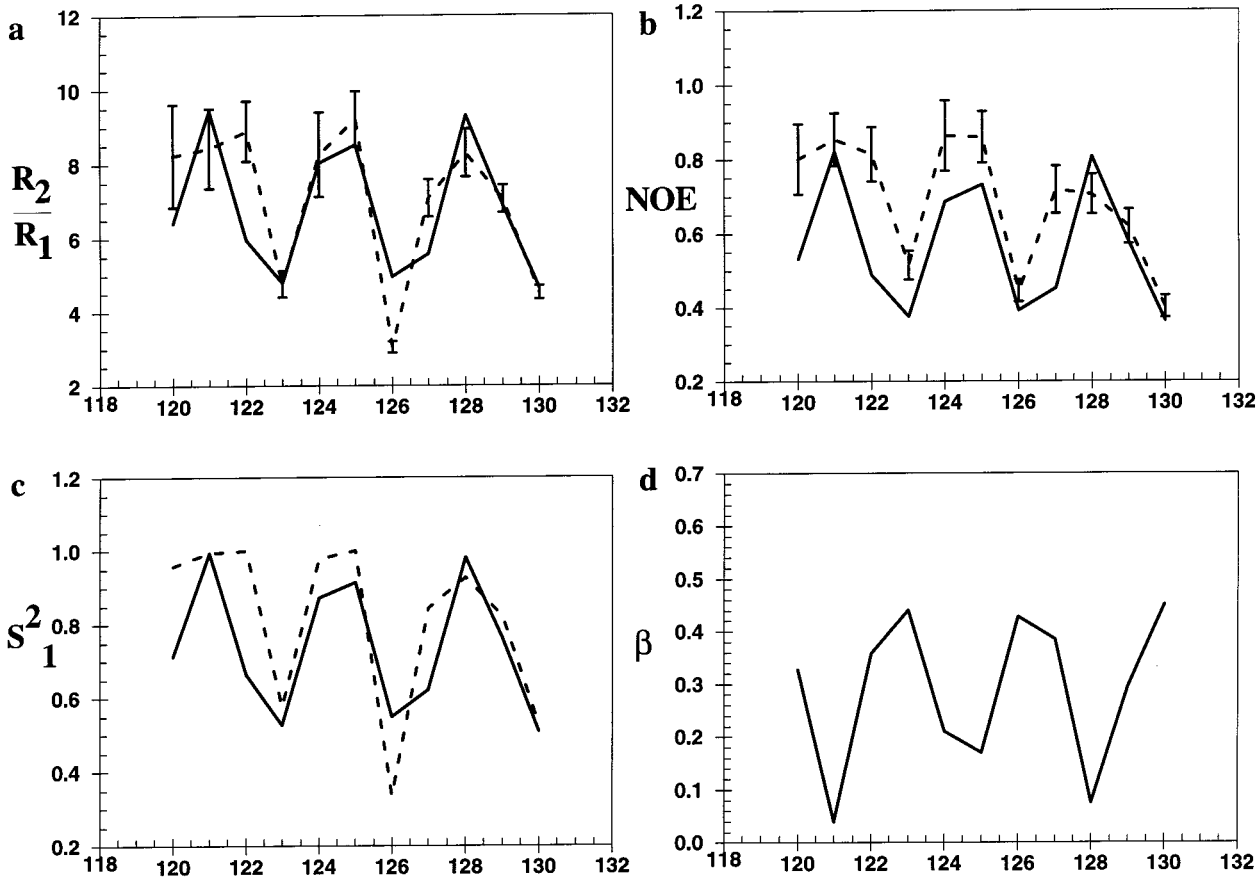

FIGURE 9: Fits of the relaxation parameters of the C-terminal helix using an explicit geometric model. (a) Relaxation rate ratios R_2/R_1 for the 11 residues treated from the C-terminal helix assuming reorientation of the structural element as a rigid body rotation. The experimental and simulated values using free rotation about an axis are indicated with dashed and solid lines, respectively. The fit using a restrained rotation is indistinguishable from the free rotation fit. (b) Experimental and simulated NOEs (plotted as in panel a). (c) Effective S_1^2 from the Lipari−Szabo fit (dashed line) and optimized (solid line) using eq 3. (d) Effective angle β (rad) of the individual vectors with respect to the axis of rotation derived from the fit. Both fits provide significantly better fits than for a rigid helix which undergoes no angular reorientation.

for its location and therefore for its absence of mobility. Our results suggest however that the lipoamide arm is not free to move in the solvent, and the location observed by radiocrystallography is conserved in solution, at least for the part of the cofactor close to the amide bond.

In contrast to these results, only very small chemical shift differences were observed between the unlipoylated and lipoylated forms of the lipoyl domains of the E2 protein (*44*, *45*) from the 2-oxoacid dehydrogenase complexes. The most important variations (^{1}HN > 0.1 ppm) were found only for residues close to the lipoylation site (*45*). This was interpreted by the authors as an indication of free swinging lipoyl groups in the 2-oxoacid dehydrogenase complexes. Thus, the lipoamide arm in the H protein seems to be less exposed and more constrained than in the E2 protein. This idea is further supported by the backbone dynamics analysis of Hox and Hapo. A mobility decrease of the region of Asp33−Leu35 is observed in the lipoylated form by comparison with the apoprotein (panels a and b of Figure 8) and is possibly due to close interaction of the arm with these residues. Indeed, it has been reported by others that residues involved in interactions with the ligand often exhibit increased order parameters (*46*, *47*). However, as the lipoamide arm is not labeled, ^{13}C relaxation measurements cannot be performed, and therefore, no quantitative information is available about the mobility in particular for the extremity of the cofactor.

These results show that the model of a swinging arm proposed for the other lipoate-containing complexes is not acceptable for the glycine decarboxylase complex. Moreover, as the methylamine group is locked inside the cleft of the H protein, it is conceivable that the T protein, once anchored to the Hmet protein, not only brings its cofactor H_4FGlu_n in close contact with the methylamine group as suggested by Cohen-Addad et al. (*7*) but also must destabilize the loaded form by unlocking the arm so that the methylene group can be amenable to direct nucleophilic attack by the tetrahydrofolate−polyglutamate. Indeed, preliminary experiments indicated that when the T protein was added to the Hmet solution in a stoechiometric amount it led to a strong increase in the rate of the methylamine unloading, a process which was shown to be pH- and temperature-dependent (L. Guilhaudis, unpublished results).

Comparison of the Three Forms of the H Protein in Solution. It is reasonable to suppose that some specific molecular recognition between each form of the H protein and its reaction partner protein is essential to the enzymatic activity of the complex, implying structural changes between the three forms. Although the global structure of the protein remains unchanged in the unlipoylated, oxidized, and methylamine-loaded crystallographic structures of the H protein (*6*, *7*, *13*), the two molecules are easily separated by ion exchange chromatography (*14*), implying a difference in the

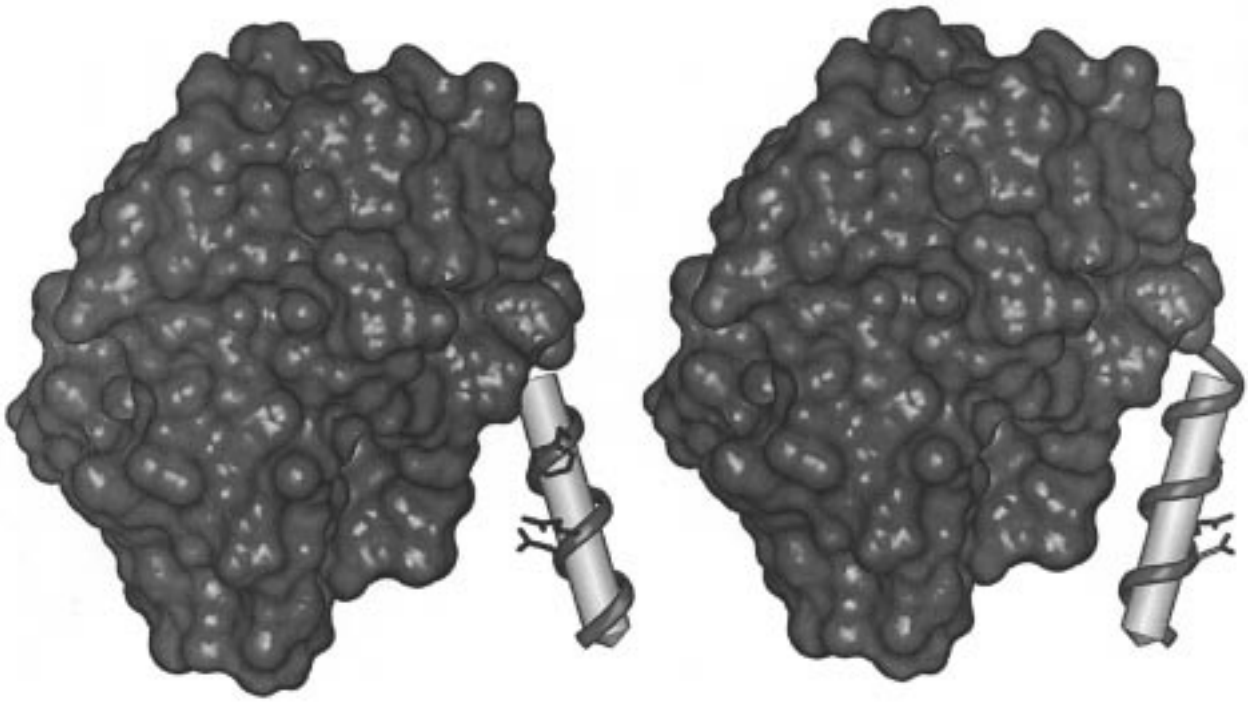

FIGURE 10: Model of reorientation of the C-terminal helix in the Hapo form. The axis of rotation derived from the fit is denoted by a solid line. The C-terminal is represented by a ribbon. The figure was produced using Insight97 (MSI Technologies).

apparent electric charge. To further investigate possible differences between the forms, we compared their behavior in solution using chemical shift variation and ^{15}N relaxation.

The analysis of chemical shift variations between the free and the ligand-bound forms of a protein is a sensitive technique for both localizing the ligand binding site and identifying significant structural changes between the two forms. Apart from variations near the lipoylation site and the region of Leu35-Gly36 assigned to the interaction with the lipoamide arm, we observed unexpected changes for residues Ser12, His13, and Glu14 between the Hapo and Hox forms (Figure 5 and panels a and b of Figure 6). This observation remains unexplained as the Glu14 side chain and the dithiolane moiety of the lipoamide arm are too far apart for direct interaction. It is possible that these shifts are related to changes in the hydrogen bond network or side chain positions within the hydrophobic pocket.

The chemical shift variations between the loaded and the oxidized forms are much more numerous than those found between the apo and oxidized proteins (panels c and d of Figure 6). The majority of these variations are localized in the hydrophobic pocket or near the lipoylation region and therefore correspond to the interaction site of the loaded lipoamide arm. However, chemical shift differences are also found in regions of the protein which are quite far from the arm, for instance, in the region of Val79−Thr84 (Figure 6d). This is surprising as no structural changes are observed between the crystallographic structures which could account for these differences.

The dynamic behavior of the H protein due to the presence and absence of lipoamide was investigated using ^{15}N relaxation. The model-free analysis shows that the H protein is a relatively rigid molecule in its three forms, and that the overall correlation times for the three forms of the H protein are similar. A highly flexible surface loop (Gly20−Val22) is present in the three forms, and the similarity of this local parametrization from the different data sets provides a reference for the level of confidence available in the data. As has often been observed, the flexible regions do not correlate well with high *B*-factors in the relevant crystal structures.

Significant variation was observed in the picosecond to nanosecond dynamics of the different forms of the protein. While there are no significant changes in the nonbond contacts implicating the peptide chain which could explain the differential mobility, possible mechanisms for the observed differences can be proposed on the basis of the dynamic behavior of the existing interactions.

The dynamic parameters reveal that the Hapo form exhibits much more flexibility on a nanosecond time scale than either of the other two forms, and particularly when compared to the loaded molecule. Large amplitude, slow motions are present on both sides of the cavity formed by the ligand-bearing β strand (Gly57−Asp67) and the short helix region (Asp29−Leu35), implying a destabilization of this pocket due to the absence of the ligand. The C-terminal helix is also found to be highly flexible. In the Hmet form, the region surrounding the lipoate arm is completely restricted and the C terminus helix is comparatively rigid.

The destabilization of the pocket in the unlipoylated form is not surprising given the loss of many nonbond contacts observed between the lipoate arm and residues in this region (*7*) in the lipoylated forms. The accompanying flexibility of the C-terminal helix may also be a consequence of the instability of this cavity. The short helix region (Asp29−Leu35) forming the back of the pocket contains two of the three histidine residues forming the interface with the charged face of the C-terminal helix (Figure 11). In all three crystal structures, the His30 N^{ξ} is positioned favorably to form a hydrogen bond with the Asp128 O^{δ} while the Thr28 O^{γ} can form a hydrogen bond with the Tyr120 O^{ξ}. A hydrogen bond interaction has also been observed between the His13 and

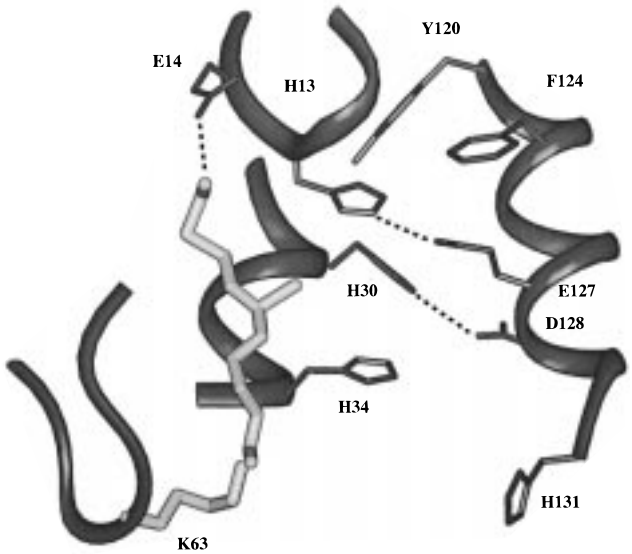

FIGURE 11: Ribbon diagram showing the H-bond network implicated in the C-terminal helix stabilization. The lipoyl−lysine arm is light gray, and the side chains of residues are dark gray. The H-bonds connecting the C-terminal helix to the hydrophobic cleft are denoted by dashed lines. The coordinates were taken from the X-ray structure of the Hmet protein (*6*).

the S6 of the lipoamide arm, mediated by a water molecule (*7*), while the His13 N^{ξ}···Glu127 O^{ϵ} hydrogen bond stabilizes the position of the C-terminal helix. The mobility of the Asp29−Leu35 helix, or the absence of the methylamine group interaction with Glu14 and Ser12, could provide mechanisms for the observed destabilization of the C-terminal helix, which itself is far from the ligand arm.

The dynamic behavior of the C-terminal helix is intriguing. The presence of vectors exhibiting large amplitude (low S^2) nanosecond time scale motions periodically along the helix suggests one of two possible models. The first supposes that the helix unwinds locally on one side, possibly cooperatively, due to the dynamic interactions of the charged and aromatic side chains with the main body of the protein. These may destabilize the hydrogen bonds of the associated residues, as the affected residues all have nonbonded side chain interactions with the rest of the protein, resulting in the large amplitude motions implied by the relaxation measurements. A second model proposes that the helix remains intact, but undergoes a reorientation due to the destabilization of the "tethering" hydrogen bonds on one side of the helix. While we are unable to distinguish between the collective rotation or cooperative unfolding models without further relaxation measurements, it seems probable that this dynamic behavior is due to the destabilization of interactions with the rest of the protein. The observation that an anisotropic global rotational diffusion tensor can reproduce the relaxation measurements of the rest of protein but not the C-terminal helix provides further evidence for the inherent reorientational freedom of this structural motif.

The mobility of the Hox is also interesting in light of the different dynamic behavior of the Hmet and Hapo forms of the protein. The observed flexibility of the pocket in the Hapo form is less pronounced in this form; in particular, the mobility of the Asp29−Leu35 residues is no longer observed, possibly due to the presence of nonbond contacts of the lipoamide group with the His34 (*6*), and the hydrogen bond of the Lys63 N^{ϵ} with the His34 carboxyl oxygen. The latter may not be present in the Hapo form due to the increased freedom of the free lysine NH_3 group. A destabilization of the C-terminal helix is observed in the Hox which is less pronounced than in the Hapo form (the Phe123 does not exhibit large scale slow motions). This implies that the interaction of the methylamine group with Ser12−Glu14 and the His13 N^{ξ}···Glu127 O^{ϵ} interaction, or the network involving the S6, His13, and Glu127, both absent in the Hapo and Hox forms, are important for the stability of the final turns of the C-terminal helix, while the stability of the Asp29−Leu35 helix, flexible only in the Hapo form, is important for the position of the whole helix. Note that the collective motion of the helix is excluded for this form of the protein.

Despite the structural similarity of the three forms of the protein, their dynamic behavior is thus significantly different. Local changes due to perturbed nonbond contacts are observed, while the possible disruption of long range hydrogen bonding and hydrophobic interactions between the main body of the protein and the C-terminal helix may explain the greater flexibility of this motif. The exact function of this helix remains unknown; however, it is possible that the position and inherent flexibility of the motif are important in the interaction interface between the H protein and its various partners. The added mobility of the highly charged C-terminal helix may explain the differential electrophoretic behavior of the oxidized and loaded forms, especially if the protonation states of the interacting histidines and glutamate 127 are affected.

CONCLUSION

In conclusion, our results demonstrate that, for Hmet, the lipoic cofactor is located in the cleft of the H protein in solution. This implies that the model of a freely swinging arm proposed for other lipoate-containing proteins is not valid for the GDC. The absence of the cofactor does not induce large scale stuctural changes but leads to a significantly different dynamic behavior. In particular, the differential mobility of the C-terminal helix may provide an explanation for the change in the isoelectric point of the oxidized and loaded forms of the protein (*14*).

ACKNOWLEDGMENT

We thank Dr. Michel Jaquinod (Laboratoire de Spectrométrie de masse des Protéines, Institut de Biologie Structurale "Jean-Pierre Ebel") for performing the mass spectrometry analysis. We also thank Virginie Gueguen for lipoylation experiments and Agnes Jourdain for her technical assistance in the overexpression and purification of the different H proteins. Special thanks to Magali Faure and Claudine Cohen-Addad for helpful discussions.

SUPPORTING INFORMATION AVAILABLE

Six tables giving the values and uncertainties of the experimentally determined R_1, R_2, and NOE values and of model-free parameters calculated for each form of the H protein. This material is available free of charge via the Internet at http://pubs.acs.org.

REFERENCES

1. Kikuchi, G., and Hiraga, K. (1982) *Mol. Cell. Biochem. 45*, 137−149.
2. Douce, R., and Neuburger, M. (1989) *Annu. Rev. Plant Physiol. Plant Mol. Biol. 40*, 371−414.
3. Oliver, D. J., Neuburger, M., Bourguignon, J., and Douce, R. (1990) *Plant Physiol. 94*, 833−839.
4. Douce, R., Bourguignon, J., Macherel, D., and Neuburger, M. (1994) *Biochem. Soc. Trans. 22*, 184−188.
5. Pares, S., Cohen-Addad, C., Sieker, L., Neuburger, M., and Douce, R. (1994) *Proc. Natl. Acad. Sci. U.S.A. 91*, 4850−4853.
6. Pares, S., Cohen-Addad, C., Sieker, L., Neuburger, M., and Douce, R. (1995) *Acta Crystallogr. D51*, 1041−1051.
7. Cohen-Addad, C., Pares, S., Sieker, L., Neuburger, M., and Douce, R. (1995) *Nat. Struct. Biol. 2*, 63−68.
8. Reed, L. J. (1974) *Acc. Chem. Res. 7*, 40−46.
9. Berg, A., Vervoort, J., and de Kok, A. (1996) *J. Mol. Biol. 261*, 432−442.
10. Ambrose, M. C., and Perham, R. N. (1976) *Biochem. J. 155*, 429−432.
11. Grande, H. J., Van Telgen, H. J., and Veeger, C. (1976) *Eur. J. Biochem. 71*, 509−518.
12. Perham, R. N. (1991) *Biochemistry 30*, 8501−8512.
13. Macherel, D., Bourguignon, J., Forest, E., Faure, M., Cohen-Addad, C., and Douce, R. (1996) *Eur. J. Biochem. 236*, 27−33.
14. Neuburger, M., Jourdain, A., and Douce, R. (1991) *Biochem. J. 278*, 63−68.
15. Morris, W. M., Reed, K. E., and Cronan J. E. (1994) *J. Biol. Chem. 269*, 16091−16100.
16. Green, D. E., Morris, T. W., Green, J., Cronan, J. E., and Guest, J. (1995) *Biochem. J. 309*, 853−862.
17. Gueguen, V., Macherel, D., Neuburger, M., Saint-Pierre, C., Jacquinod, M., Gans, P., Douce, R., and Bourguignon, J. (1999) submitted for publication in *J. Biol. Chem.*
18. Neuburger, M., Pietre, E., Polidori, A., Faure, M., Jourdain, A., Bourguignon, J., Douce, R., and Pucci, B. (1999) (manuscript in preparation).
19. Braunschweiler, L., and Ernst, R. R. (1983) *J. Magn. Reson. 53*, 521−528.
20. Davis, D. G., and Bax, A. (1985) *J. Am. Chem. Soc. 107*, 2820−2821.
21. Jeener, J., Meier, B. H., Bachmann, P., and Ernst, R. R. (1979) *J. Chem. Phys. 71*, 4546−4553.
22. Macura, S., Hyang, Y., Suter, D., and Ernst, R. R. (1981) *J. Magn. Reson. 43*, 259−281.
23. Bodenhausen, G., and Ruben, D. J. (1980) *Chem. Phys. Lett. 69*, 185−188.
24. Marion, D., Driscoll, P. C., Kay, L. E., Wingfield, P. T., Bax, A., Gronenborn, A. M., and Clore, G. M. (1989) *Biochemistry 28*, 6150−6156.
25. Piotto, M., Saudek, V., and Sklenar, V. (1992) *J. Biomol. NMR 2*, 661−665.
26. Plateau, P., and Guéron, M. (1982) *J. Am. Chem. Soc. 104*, 7310−7311.
27. Marion, D., Ikura, M., Tschudin, R., and Bax, A. (1989) *J. Magn. Reson. 85*, 393−399.
28. Shaka, A. J., Barker, P. B., and Freeman, R. (1985) *J. Magn. Reson. 64*, 547−552.
29. Wishart, D. S., Bigam, C. G., Yao, J., Abildgaard, F., Dyson, H. J., Oldfield, E., Markley, J. L., and Sykes, B. D. (1995) *J. Biomol. NMR 6*, 135−140.
30. Morris, G. A., and Freeman, R. (1979*) J. Am. Chem. Soc. 101*, 760−762.
31. Burum, D. P., and Ernst, R. R. (1980) *J. Magn. Reson. 39*, 163−168.
32. Farrow, N. A., Muhandiram, R., Singer, A. U., Pascal, S. M., Kay, C. M., Gish, G., Shoelson, S. E., Pawson, T., Forman-Kay, J. D., and Kay, L. E. (1994) *Biochemistry 33*, 5984−6003.
33. Kay, L. E., Keifer, P., and Saarinen, T. (1992) *J. Am. Chem. Soc. 114*, 10663−10665.
34. Palmer, A., Skelton, N. J., Chazin, W. J., Wright, P. E., and Rance, M. (1992) *Mol. Phys. 75*, 699−711.
35. Shaka, A. J., Keeler, J., and Freeman, R. (1983) *J. Magn. Reson. 53*, 313−340.
36. Cordier, F., Caffrey, M., Brutscher, B., Cusanovich, M., Marion, D., and Blackledge, M. (1998) *J. Mol. Biol. 281*, 341−361.
37. Lipari, G., and Szabo, A. (1982) *J. Am. Chem. Soc. 104*, 4546−4558.
38. Lipari, G., and Szabo, A. (1982) *J. Am. Chem. Soc. 104*, 4559−4570.
39. Clore, G. M., Szabo, A., Bax, A., Kay, L. E., Driscoll, P. C., and Gronenborn, A. M. (1990) *J. Am. Chem. Soc. 112*, 4989−4991.
40. Mandel, A. M., Akke, M., and Palmer, A. G. (1995) *J. Mol. Biol. 246*, 144−163.
41. Woessner, D. E. (1962) *J. Chem. Phys. 37*, 647−654.
42. Blackledge, M., Cordier, F., Dosset, P., and Marion, D. (1998) *J. Am. Chem. Soc. 120*, 4538−4539.
43. Woessner, D. E. (1962) *J. Chem. Phys. 36*, 1−4.
44. Dardel, F., Laue, E. D., and Perham, R. N. (1991) *Eur. J. Biochem. 201*, 203−209.
45. Berg, A., De Kok, A., and Vervoort, J. (1994) *Eur. J. Biochem. 221*, 87−100.
46. Nicholson, L. K., Kay, L. E., Baldisseri, D. M., Arango, J., Young, P. E., Bax, A., and Torchia, D. A. (1992) *Biochemistry 31*, 5253−5263.
47. Akke, M., Shelton, N. J., Kîrdel, J., Palmer, A. G., III, and Chazin, W. J. (1993) *Biochemistry 32*, 9832−9844.

BI990422P